Theor Chem Acc (2009) 123:353–364
DOI 10.1007/s00214-009-0530-3

REGULAR ARTICLE

Topological models of magnetic field induced current density field in small molecules

Stefano Pelloni · Paolo Lazzeretti · Riccardo Zanasi

Received: 18 December 2008 / Accepted: 4 February 2009 / Published online: 26 February 2009

Abstract Three-dimensional models of the quantum mechanical current density induced in the electrons of LiH, BeH_2, and CO_2 molecules by a magnetic field applied perpendicularly to the bond axis have been constructed at the Hartree-Fock level of accuracy. The topological features of the current density vector field are described via a stagnation graph that contains the isolated points and the lines at which the current vanishes, and by planar and spatial streamline plots.

1 Introduction

In the hydrodynamic approach to non-relativistic quantum mechanics first proposed by Madelung [1], allowing for an optico-mechanical analogy and for the definitions of charge density and charge current density introduced slightly earlier by Schrödinger [2], a complex wave function is written in semiclassical form, $\Psi = R\exp(iS/\hbar)$. $R(\mathbf{r},t)$ is the real-valued amplitude and the phase $S(\mathbf{r},t)/\hbar$ corresponds to the eikonal of geometrical optics [3–5]. By substituting this Ψ into the time-dependent Schrödinger equation, a set of hydrodynamic relationships is obtained, i.e., a continuity equation and a modified Hamilton–Jacobi equation of motion [6, 7], which describe quantum trajectories of particle flow.

Further improvements were proposed by Landau [8], London [9], and Bohm, in two extensive papers [10, 11] that yield the conceptual basis for a causal interpretation of quantum theory [12–17]. By analogy with classical electrodynamics, the quantum mechanical probability current density is defined via the relationship $\mathbf{j} = \gamma\mathbf{v}$, where $\gamma(\mathbf{r},t) = R^2(\mathbf{r},\ t)$ is the probability density, and $\mathbf{v}(\mathbf{r},t) = 1/m(\nabla S - q/c\mathbf{A})$ is the Madelung-London-Landau local average velocity of a particle with mass m and charge q, in the presence of a vector potential $\mathbf{A}(\mathbf{r},t)$.

As a matter of fact, the hydrodynamic formulation provides an alternative foundation of quantum mechanics of great historical and epistemological value for discussing the transition between classical and quantum mechanics [18].[1] Moreover it turns out to be very appealing for several applications [19−31], and quite effective for understanding molecular magnetic response, which can be rationalized via the electronic current density $\mathbf{J}^{\mathbf{B}}$ field induced by an external magnetic field with flux density $\mathbf{B}$.

The practical advantages of using a vector function of position in $\mathbb{R}^3$ real space, instead of a complex wave

Dedicated to the memory of Professor Oriano Salvetti and published as part of the Salvetti Memorial Issue.

Electronic supplementary material The online version of this article (doi: 10.1007/s00214-009-0530-3) contains supplementary material, which is available to authorized users.

S. Pelloni · P. Lazzeretti (✉)
Dipartimento di Chimica dell'Università degli Studi di Modena, Via Campi 183, 41100 Modena, Italy
e-mail: lazzeret@unimo.it
URL: http://theochem.chimfar.unimo.it

R. Zanasi
Dipartimento di Chimica dell'Università degli Studi di Salerno, Via Ponte don Melillo, 84084 Fisciano (SA), Italy

[1] Bohm and Peat [18] emphasize the importance of the intrinsic wave-particle dichotomy characterizing the Hamilton-Jacobi theory as a classical root of quantum mechanics. According to these authors, Hamilton had already developed the optico-mechanical similarity to such an extent that he might have put forward a wave mechanics analogous to wave optics. Therefore they speculate that, allowing for the Hamilton-Jacobi formulation in the regime of short wavelength, a wave mechanics might be derived from the classical mechanics of the nineteeth century, just as a wave optics is derived from geometric optics.

function which depends on $3n$ space-spin coordinates for analyzing the magnetic properties of a molecule with n electrons, are shown in early papers on diatomic [32–35] and polyatomic molecules [36–39], and in recent studies [40–51].

Understanding structure and properties of quantum mechanical current density fields induced by an applied magnetic perturbation in a molecule is per se theoretically appealing. A number of studies demonstrate that it is also very useful for solving problems and answering basic questions. What does $\mathbf{J}^{\mathbf{B}}$ look like in the outer and inner regions? How are domains characterized by different regime related to one another? What about the requirement of continuity and charge conservation? To what extent are measurable properties, for instance, magnetizability and magnetic shielding of the nuclei, affected by the global and local distribution of currents? Are there practical and effective tools providing a realistic and concise description of the electron flow in three-dimensional space?

Some authors adopt a simple representation by a set of arrows [52–58] to visualize essential features of the quantum mechanical $\mathbf{J}^{\mathbf{B}}$ vector field on selected plot planes perpendicular to $\mathbf{B}$, which however is, in most cases, insufficient to explain the magnetic properties of small-size molecules, and sometimes misleading for rationalizing magnetotropicity of more complicated systems.

In general, the quantum mechanical $\mathbf{J}^{\mathbf{B}}$ is not perpendicular to the applied stationary field unless constrained to be so by symmetry. While the component parallel to $\mathbf{B}$ does not contribute to the diagonal components of the magnetic susceptibility and nuclear magnetic shielding tensors, it must be taken into account, first and foremost to satisfy the continuity condition $\nabla \cdot \mathbf{B} = 0$. Secondly, it is indispensable for the analysis of the phase portraits. It should therefore be emphasized that the three-dimensional structure of magnetically induced current density fields is actually needed for interpreting molecular magnetism.

Compact topological models based on stagnation graphs, and associated streamline and modulus maps, constitute the best instruments available nowadays to come to grips with the spatial features of complicated current density fields. The present paper aims at providing these models for a set of small molecules, LiH, BeH_2, CO_2.

The basic aims of the present research on small molecules are (1) to visualize elementary spatial patterns of magnetic field induced quantum mechanical electron current density which are expected to be transferable from one system to another (2) to construct simple and accurate models which underlie the elucidation of magnetic response of more complex systems, and help obtain a physical understanding of unusual properties, e.g., electronic anapole moments which so far have not been detected.

2 Computational procedures

Early studies adopted coupled Hartree-Fock (CHF) methods, a common origin (CO) for the vector potential, gaugeless basis sets, and separated maps for streamlines and moduli [32–39]. Displays of the $\mathbf{J}^{\mathbf{B}}$ field on a plane were obtained via arrows of length proportional to the local modulus [52–54], employing the individual gauge for localized orbitals (IGLO) method [54, 59–61]. Bulging arrows are also widely employed [55, 56].

A gauge-including magnetically induced current (GIMIC) method using the arrow representation has been implemented at the coupled-cluster singles and doubles (CCSD) level, and it has been applied to a series of molecules and ions [62–64]. 4-Component relativistic calculations of the magnetically induced current density have been reported for the group 15 heteroaromatic compounds [65].

A major advancement in the representation of $\mathbf{J}^{\mathbf{B}}$ fields via high-quality displays was made by Keith and Bader [40–44], who developed a theoretical procedure referred to as continuous set of gauge transformations (CSGT). Their computational scheme, based on numerical integration, has been coded in the GAUSSIAN package [66].

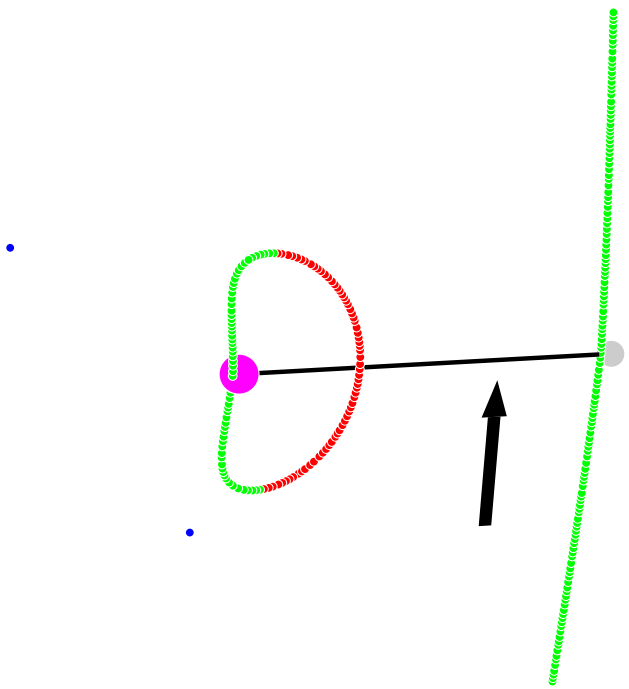

Fig. 1 Perspective view of the stagnation graph of the LiH molecule for a magnetic field (represented by a *big black arrow* in all the figures) directed perpendicular to the bond. *Green* (*red*) *stagnation lines* denote diamagnetic (paramagnetic) vortices. The stagnation loop and two off-axis conjugated saddle-node (3,±1) stagnation points (represented in *blue*) indicate toroidal flow in the basin of Li atom. The SG can be magnified and rotated for better inspection (see Footnote 3)

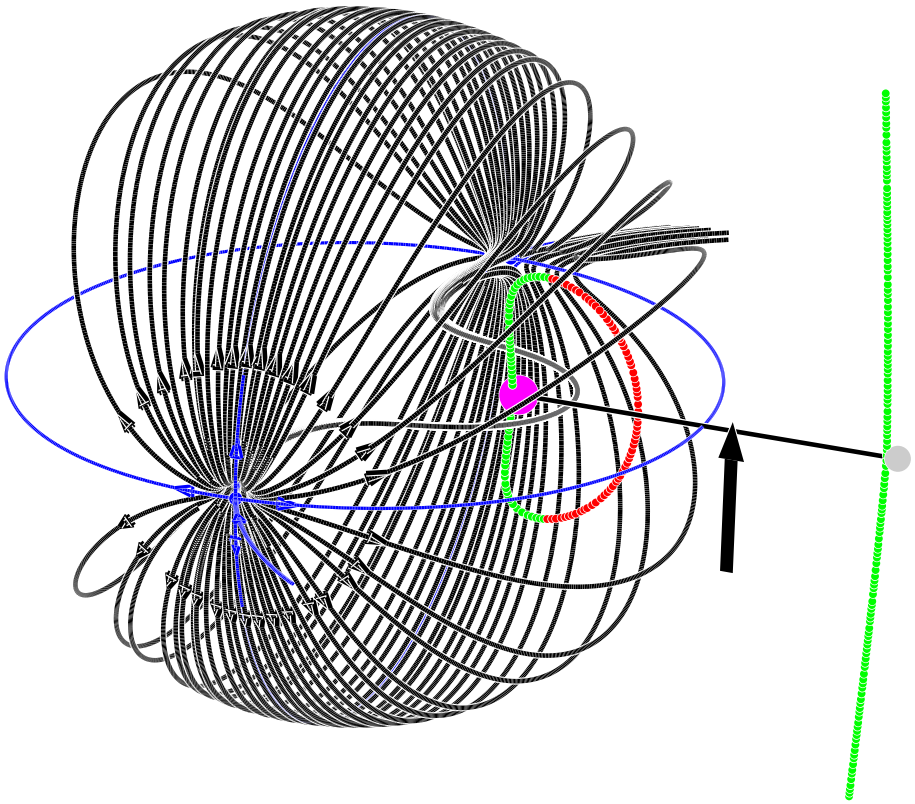

Fig. 2 Perspective view of the toroidal flow in the basin of the Li atom in the LiH molecule for a magnetic field directed perpendicular to the bond. This pattern can be magnified and rotated (see Footnote 3) for better inspection. All the streamlines flow through the centre and around the sides of the stagnation loop containing one green and one red segment. The (3,1) saddle-node, observed in the foreground as a source, is connected to its conjugated (3,−1) (sink) partner lying behind the torus by black trajectories. A blue closed asymptotic line defines the intersection of the separatrix containing the torus with the plane of the nuclei perpendicular to the applied field. On this plane, the (3,±1) points look like saddles. The other homoclinic blue line joining the (3,±1) points lies on a plane normal to the bond axis. A wavy asymptotic line, which connects the (3,±1) points passing inside the stagnation loop, is best observed in Fig. 3

An alternative approach relying on an analytical version of the method proposed by Keith and Bader [40, 41], and connected with procedures proposed by Geertsen [67–69], allows for a continuous transformation of the origin of the current density that formally sets to zero the diamagnetic contribution (CTOCD-DZ) [70]. However, the CTOCD-DZ method suffers from slow convergence of calculated properties to the HF limit. It should carefully be applied by adopting large basis sets, as it overestimates paramagnetism [40, 71] and gives a wrong description of electron currents about nuclei heavier than hydrogen's [48, 51].

A practical variant referred to as DZ2, based on damping functions and numerical integration, is more effective and provides good displays of current density and accurate predictions of magnetic properties with medium size basis sets [40, 72]. The CTOCD-DZ2 method was preferably used to describe current density vector fields in recent applications, see [45–51] for details.

Van Duijneveldt's (13s8p/8s) basis sets [73] of primitive Gaussian functions were employed as substrata in this study. The polarization functions used are specified in the section of supplementary material. For consistency, molecular geometries were fully optimized at the HF level using the same basis sets. The CHF scheme implemented in the SYSMO code [74] was applied within the conventional CO method and CTOCD-DZ2 procedures [58, 72].

The models developed in the present study are of near HF quality, as proven by sum rules for gauge invariance and charge conservation, and virtual identity of magnetic properties estimated by different computational schemes, see the supplementary material available. Electron correlation might bias the results to some extent [62–64].

3 Spatial current models

The essential features of a $\mathbf{J}^{\mathbf{B}}$ field are understood via the phase portrait in the vicinity of points at which $|\mathbf{J}^{\mathbf{B}}|$ vanishes. The field $\mathbf{J}^{\mathbf{B}}(\mathbf{r})$ in the neighborhood of a stagnation point (SP) at $\mathbf{r}_0$ is described by a truncated Taylor series,

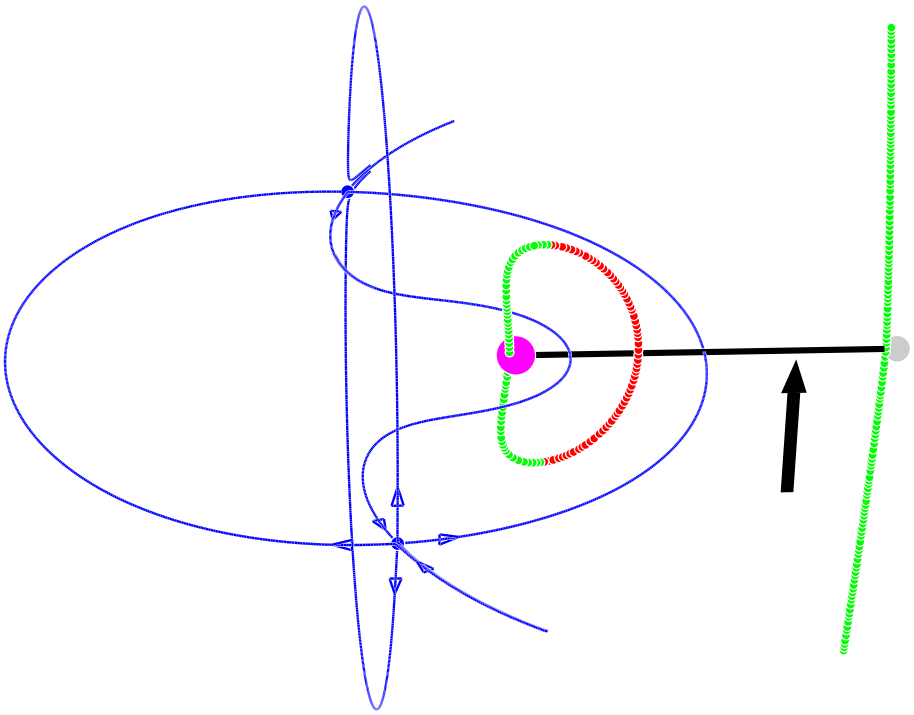

Fig. 3 Homoclinic trajectories connecting the (3,±1) saddle-nodes on the separatrix of the torus about the Li atom in the LiH molecule. The *arrows* indicate the direction of the eigenvectors of the Jacobian matrix $\nabla \mathbf{J}^{\mathbf{B}}$ at the stagnation points. An asymptotic wavy line flows across the stagnation loop, about its centre

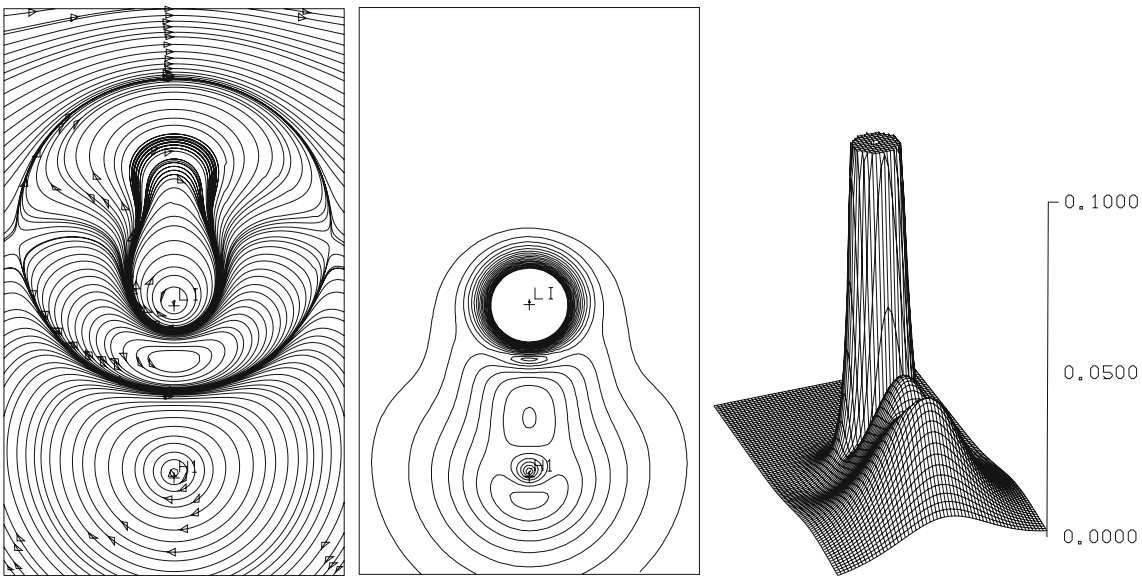

Fig. 4 The current density field for LiH for a field perpendicularly directed out of the plane containing the nuclei, with $|\mathbf{B}| = 1$ au. Diatropic (paratropic) current density is clockwise (anti-clockwise). The maximum intensity of the $\mathbf{J}^{\mathbf{B}}$ field is 0.58 au, truncated to 0.10 in the perspective view on the right. Corresponding contours start at 5.0×10^{-3} and are 5.0×10^{-3} apart

$$J_{\gamma}^{\mathbf{B}}(\mathbf{r}) = (r_{\alpha} - r_{0\alpha})\left[\nabla_{\alpha} J_{\gamma}^{\mathbf{B}}\right]_{\mathbf{r}=\mathbf{r}_0} + \frac{1}{2}(r_{\alpha} - r_{0\alpha})(r_{\beta} - r_{0\beta}) \times \left[\nabla_{\alpha}\nabla_{\beta} J_{\gamma}^{\mathbf{B}}\right]_{\mathbf{r}=\mathbf{r}_0} + \cdots \quad (1)$$

Standard tensor notation is employed, e.g., summation over repeated Greek indices is implied.

Reyn [82] showed all possible phase portraits in the proximity of an SP at $\mathbf{r}_0$ in three-dimensional flow, corresponding to canonical forms of the real 3×3 Jacobian matrix $\nabla_{\alpha} J_{\gamma}^{\mathbf{B}}(\mathbf{r}_0)$. The local regime depends on the eigenvalues of the Jacobian matrix. Accordingly, SPs are denoted via a widely adopted [41, 42, 58] (*rank, signature*)

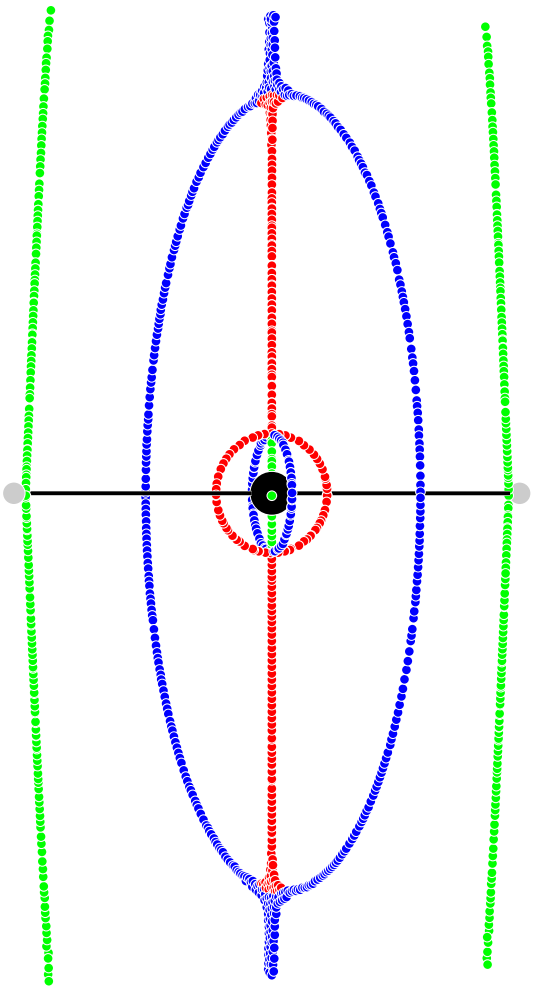

Fig. 5 Perspective view of the stagnation graph of the BeH_2 molecule in a magnetic field perpendicular to the bond axis. The central stagnation line is parallel to the applied field. The colour code is the same as in Fig. 1

label [75–77], where the rank r is defined as the number of non-vanishing eigenvalues of the Jacobian matrix and the signature s is the excess of positive over negative eigenvalues. An SP is also classified in terms of its topological index ι [79, 80].[2] The SPs may be isolated or form continuous, open or closed, paths referred to as stagnation lines (SL). Several examples have been reported in previous papers [40–51].

The three-dimensional structure of a current density vector field is described by the stagnation graph (SG), a topological tool collecting all isolated (3,±1) SPs and (2,0) SLs, which may be continuous paths of either vortex (index $\iota = +1$) or saddle (index $\iota = -1$) points. An SG illustrates branchings of an SL at (0,0) critical points. The Gomes theorem provides an index conservation condition, $\iota_0 = \sum_{k=1}^{m} \iota_k$, for a line with index ι_0 which splits into m new lines emerging from the branching point [75–78].

The critical point identifications given here are based on the calculated eigenvalues of the Jacobian matrix for three small molecules.

3.1 LiH

A pioneering investigation on the magnetically induced current density field in LiH was reported by Stevens and Lispcomb using the CHF-CO approach and a basis of Slater orbitals [32]. An extensive study by Keith and Bader [41], allowing for the CSGT method and a Gaussian basis set, gave a refined description of $\mathbf{J}^{\mathbf{B}}$ in the real space.

A spatial current model for LiH is described in Figs. 1, 2, 3, 4. The stagnation graph for a field B_x applied perpendicular to the z bond axis shown in Fig. 1 is virtually identical to that of [41]. It contains a set of (2,0) SLs lying on the $T\sigma_v(zx)$ symmetry plane (T indicates time-reversal), namely a green line, crossing the bond in the vicinity of the hydrogen nucleus and extending to the tail regions, and a closed loop formed by green and red portions, corresponding to opposite vorticity, in the basin of the Li atom. The former indicates a diamagnetic axial vortex (AV), the latter is characteristic of a toroidal vortex (TV) [81], whose presence is confirmed by a pair of blue (3,±1) conjugated SPs on either side of the bond direction, with coordinates (0,±2.75,1.90), measured in bohr, with respect to the origin in the centre of mass. These points are classified as stable and unstable saddle-nodes in the terminology of Reyn [82].

Toroidal vortices in the quantum-mechanical current density field of a single-particle system were predicted by Hirschfelder [81]. An observer in front of the nodal loop in Fig. 1 would see currents coming out from the (3,1) source point in the proximity of its centre, flowing through the centre around the sides of this loop, and entering through the (3,−1) sink behind the nodal loop. This effect can be viewed by rotating Fig. 2.[3]

The TV looks like a doughnut with a very small central hole, completely encased in a *separatrix*, that is, a surface with the shape of a (topological) sphere, separating it from the rest of the vector field. This separatrix is filled by asymptotic paths, sometimes referred to as homoclinic trajectories [77], see Fig. 3. In the streamline plot of Fig. 4, the toroidal flow is represented by two juxtaposed vortices, one diamagnetic and one paramagnetic. Their centres are

[2] The topological index ι counts the number of times that the current density vector $\mathbf{J}^{\mathbf{B}}$ rotates completely while one walks counterclockwise around a circle of radius ε, so small that $\mathbf{J}^{\mathbf{B}}$ has no zeroes inside except the SP at its center. The topological index ι of a saddle (vortex) line is -1 ($+1$). Both SPs have $(r, s) = (2, 0)$.

[3] The LINUX and WINDOWS versions of the graphic code used to obtain three-dimensional representations of the stagnation graph and current density vector field of a series of molecules can be downloaded at https://theochem.chimfar.unimo.it/VEDO3/.

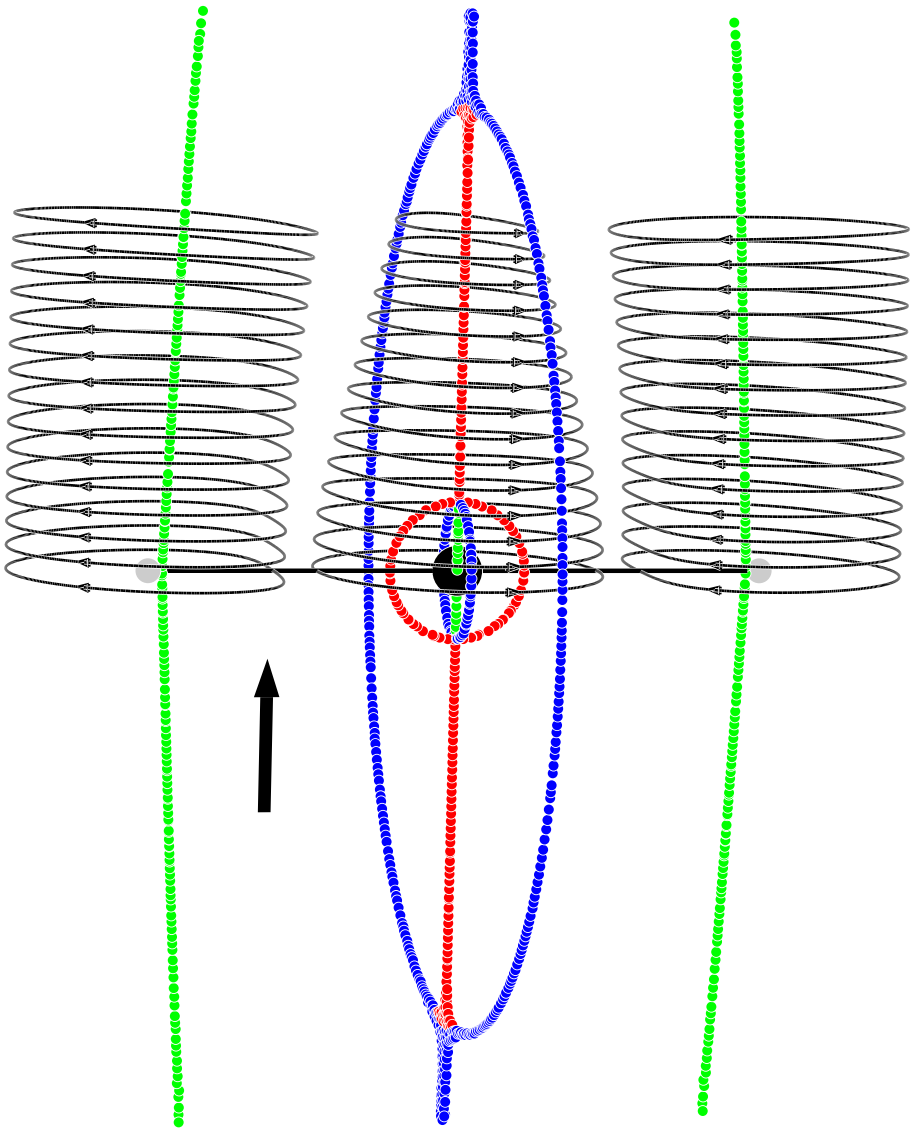

Fig. 6 Diamagnetic vortices in the basin of the hydrogen atoms and the central paramagnetic flow in the BeH_2 molecule

found at the intersection of the green and red SLs of the stagnation loop of the TV with the $\sigma_h(yz)$ plane.

The currents flowing on the surface of a torus induce an anapole moment [83] and a toroidal magnetic field with the shape of a topological circumference, confined inside this surface, see, for instance, Fig. 1 in [84]. The components of the anapole vector induced in the electrons of a molecule in the presence of a non-uniform magnetic field with uniform gradient are defined by derivatives of the molecular energy W with respect to the components of the curl $\nabla \times \mathbf{B}$, $A_\alpha = -\partial W/\partial(\nabla \times \mathbf{B})_\alpha$. The contribution depending on the electronic current density $\mathbf{J^B}$ is $\mathcal{A}_\gamma = -1/6c \int d^3r\,(r^2\delta_{\beta\gamma} - r_\beta r_\gamma) J^{\mathbf{B}}_\beta$ [84]. Toroidal vortices interact with a the gradient of non-uniform magnetic field: the curl $\nabla \times \mathbf{B}$ exerts a torque on the anapole, $K_\alpha = \epsilon_{\alpha\beta\gamma}\mathcal{A}_\beta(\nabla \times \mathbf{B})_\gamma$. The effect of toroidal flow on nuclear magnetic shielding is presently underway [85].

3.2 BeH_2

The current model for BeH_2 is illustrated in Figs. 5, 6 and 7. The stagnation graph, Fig. 5, yields a three-dimensional description of the flow induced by a magnetic field applied in the radial x direction. The SG can also be magnified and rotated by using a graphic software delivered by the authors.[3] It is characterized by five (2,0) vortical SLs crossing the z bond axis. The central stagnation path is parallel to the external field. It contains an innermost green segment, which denotes a diamagnetic vortex passing through the beryllium nucleus at the origin of the coordinate system. Such a vortex, sustained mainly by the core electrons, is also observed at the site of C and O nuclei in CO_2, see Figs. 9 and 14.

At a distance $x \approx \pm 0.54$ bohr on either side of the centre of inversion, two (0,0) branching points are observed

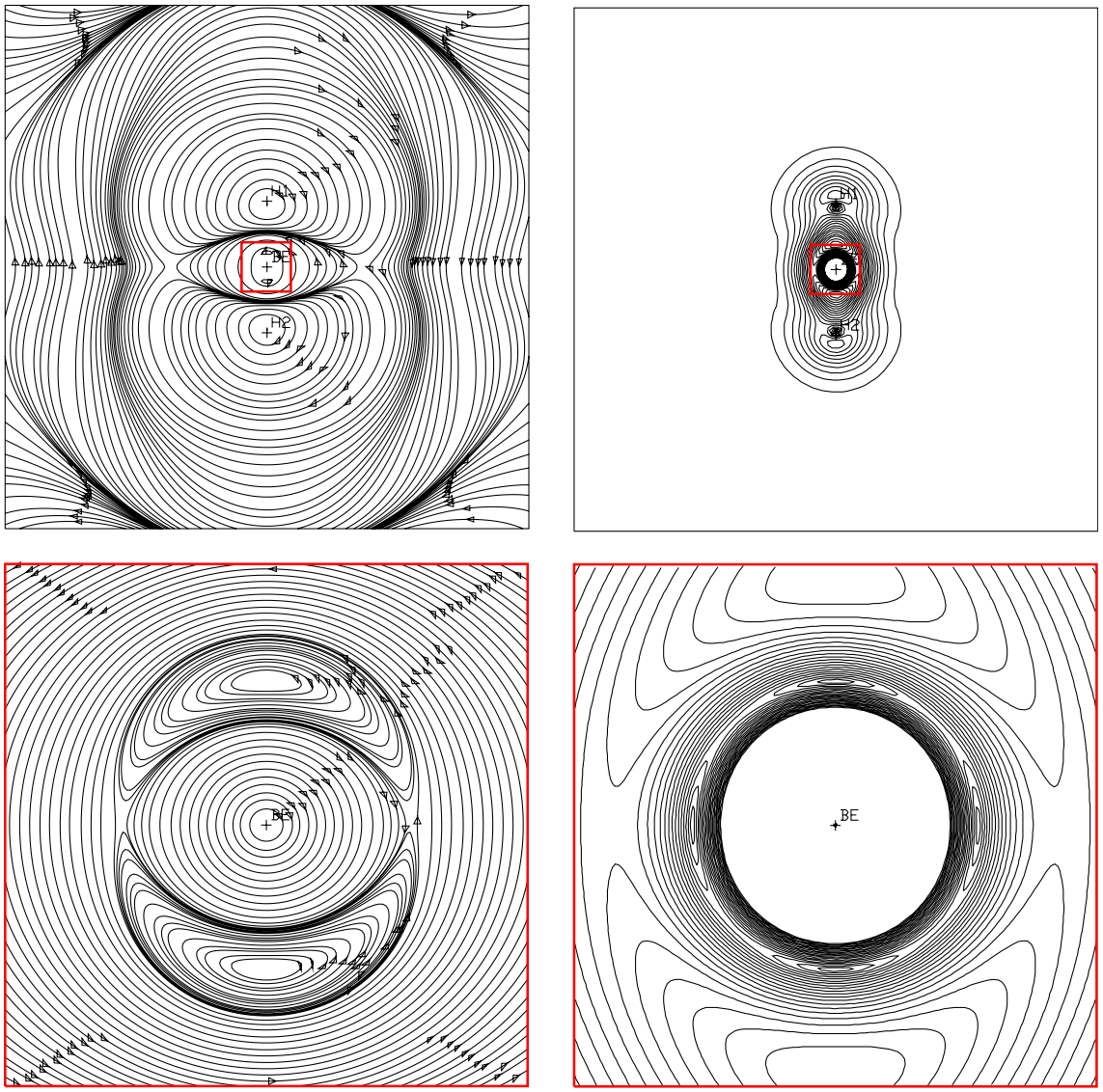

Fig. 7 The current density field for BeH_2 for a field perpendicularly directed out of the plane containing the nuclei, with $|\mathbf{B}| = 1$ au. The maximum intensity $|\mathbf{J}^{\mathbf{B}}|$ is 0.71 au, truncated to 0.10 in the contour maps on the right, which start at 5.0×10^{-3} and are 5.0×10^{-3} apart. The inset with a red frame is magnified in the bottom

in Figs. 5 and 8. The flow beyond these points is paramagnetic, as indicated by the red portions of the central SL joined to a central cage formed by (1) two paramagnetic (red) and (2) two saddle (blue) stagnation paths that lie on the symmetry planes $T\sigma_v(zx)$ and $T\sigma_v(xy)$, respectively. The index conservation condition [75–77, 86] at these (0,0) critical points is exactly fulfilled ($1 = 3 - 2$).

Two outermost saddle lines lie on the $T\sigma_v(xy)$ symmetry plane orthogonal to the bond axis and merge with the central SL on either side of the beryllium nucleus at another pair of (0,0) branching points placed at $x \approx \pm 3.7$ bohr from it. The index count gives $-1 = -2 + 1$, again fulfilling the Gomes theorem [75–77, 86].

The quality of the CHF wavefunction used to obtain the SG for BeH_2 is not sufficient to describe the field beyond the outermost (0,0) critical points. However, at a greater distance, the green (vortical diamagnetic) hydrogen SLs should merge with the central saddle path to form a single diamagnetic vortical line extending to the boundaries of the molecular domain.

The current density maps for a field perpendicularly directed out of a plane containing the internuclear axis of BeH_2 shown in Fig. 7 are fully consistent with the SG of Fig. 5 and with Fig. 6. The streamlines on a square with side 20 bohr visualize the flow in the tail regions. The central domain is magnified to observe the diamagnetic

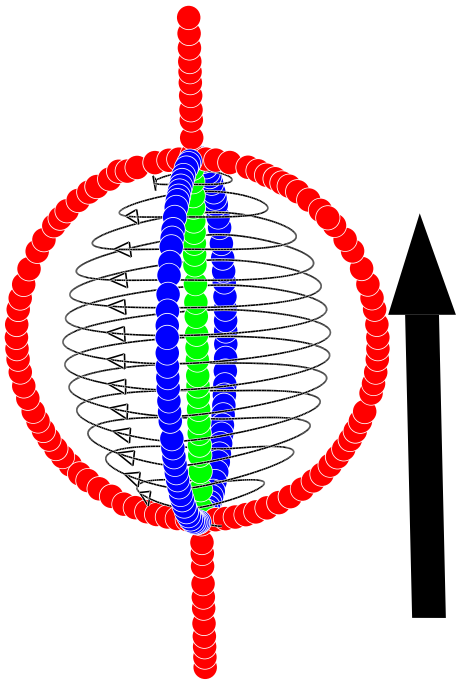

Fig. 8 Magnified view of the cage of stagnation lines about the beryllium atom and the central diamagnetic vortex in the BeH_2 molecule

vortex about the beryllium nucleus, the two paramagnetic vortices, and the two saddles at the intersection of the (2,0) SLs forming the central cage in the SG of Fig. 5 with the plot plane. The contours of the modulus $|\mathbf{J}^{\mathbf{B}}|$ show that the intensity of the current density field decays quite rapidly in the outer regions. These results are in substantial agreement with Keith and Bader [41].

3.3 CO_2

Previous investigations on the CO_2 molecules are available [41, 87]. The present study provides further information by illustrating the spatial structure of the current density field.

The current model for CO_2 is described in Figs. 9, 10, 11, 12, 13, 14. Figure 9 shows thirteen (2,0) SLs lying on the $T\sigma_v(zx)$ symmetry plane parallel to the applied field B_x and containing the internuclear z axis. The central pattern of five stagnation paths is identical to that of BeH_2 in Fig. 5, see Fig. 14. The pair of (0,0) critical points close to the carbon nucleus (at the origin of the coordinate system) is found at a distance $x \approx \pm 0.21$ bohr. A magnified view of the cage of SLs coalescing at these (0,0) points is displayed in Fig. 14. Further branching of the central SL parallel to the applied field occurs at $x \approx \pm 1.2$ and at $x \approx \pm 4.0$ bohr from the C nucleus. The index count gives $1 = 2 - 1$ for the lines merging at the outermost (0,0) points, where the central paramagnetic vortex line in the fringes of the molecule splits into a central saddle segment and two paramagnetic vortex lines connecting them.

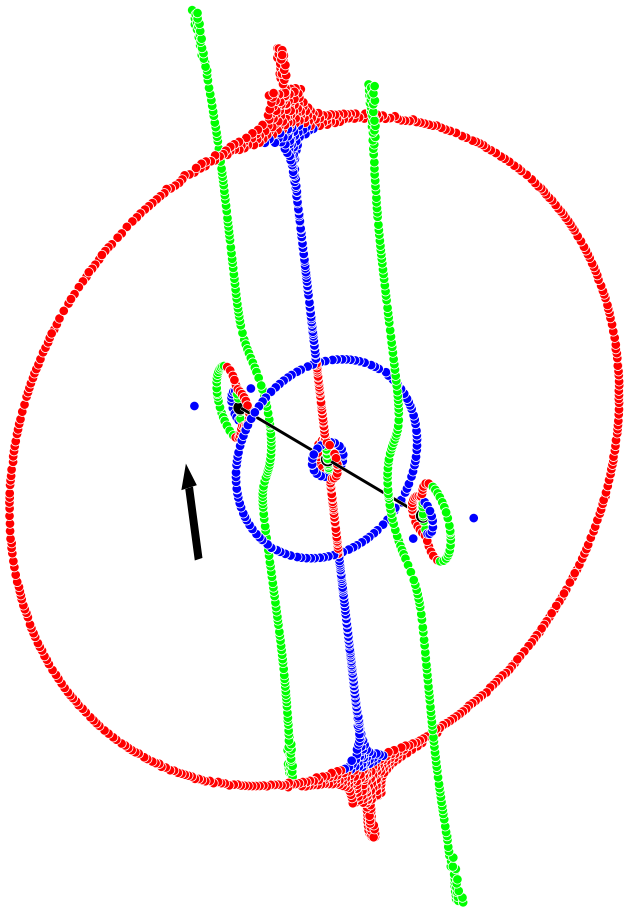

Fig. 9 Perspective view of the stagnation graph of the CO_2 molecule in a magnetic field perpendicular to the bond axis. The central stagnation line is parallel to the applied field. The colour code is the same as in Fig. 1

A set of four SLs forming two distinct continuous loops is found in the basin of each oxygen atom, see Figs. 9 and 14. The two segments of the external loop are represented in green and red to account for the local vorticity: the outermost green line crossing the bond direction on the left of Fig. 14 is vortical diamagnetic. Our findings differ from those of [41], where this segment is described as saddle-type, see Fig. 6c there. In fact, the outer loop about the oxygen nuclei in the SG of Fig. 9 indicates the typical structure of a torus [81], which is confirmed by the couple of blue (3,±1) conjugated SPs on either side of the oxygen nucleus. These points are placed at (0,±0.39,±2.59) bohr in the coordinate system adopted in this work. The smaller internal loop, formed by a saddle-line and a diamagnetic vortex-line through the oxygen nucleus, is fully enclosed within the separatrix of the torus, in the region of paramagnetic flow, as is clearly observed in Figs. 11 and 12.

Asymptotic lines originating and ending at the conjugated (3,±1) saddle-nodes are displayed in Fig. 11. They

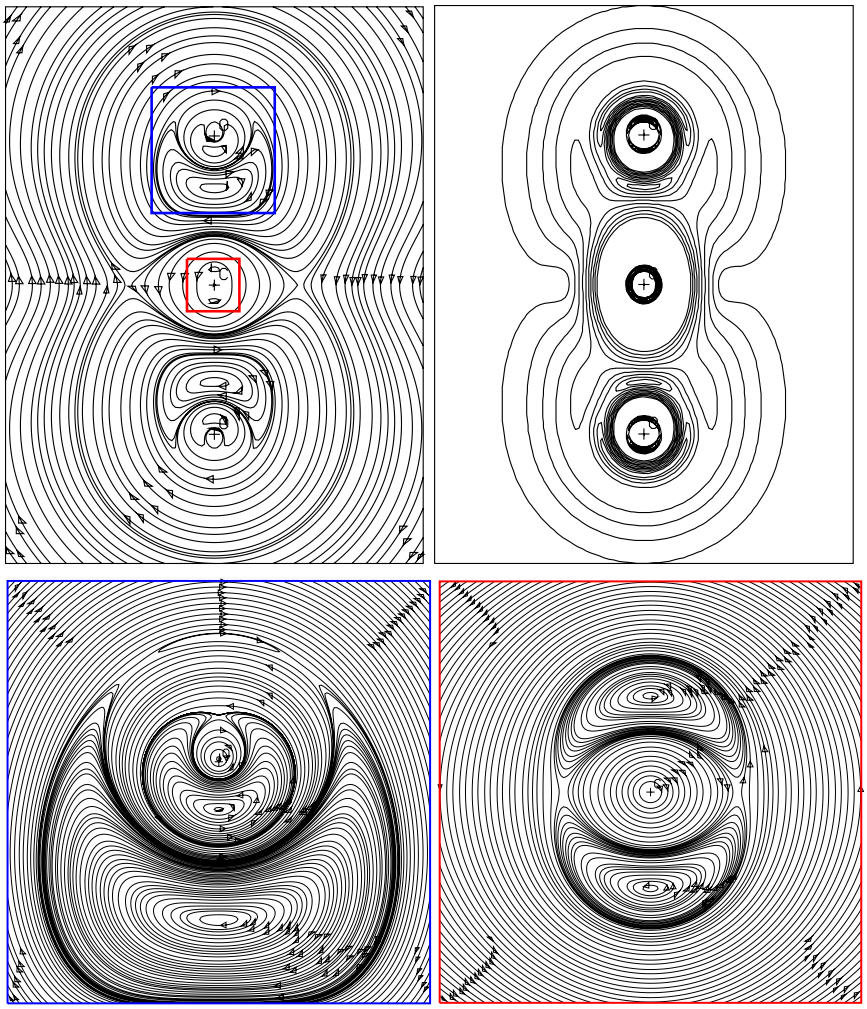

Fig. 10 The current density field for CO_2 for a field perpendicularly directed out of the plane containing the nuclei, with $|\mathbf{B}| = 1$ au. Cross-sections of the flow in the basin of an oxygen atom, showing the toroidal vortex, and about the central carbon nucleus—insets with blue and red frame, respectively, are magnified in the bottom. The maximum intensity of the $\mathbf{J}^{\mathbf{B}}$ field is 3.55 au, truncated to 0.30 in the top-right contour map, which start at 0.03 and are 0.03 apart

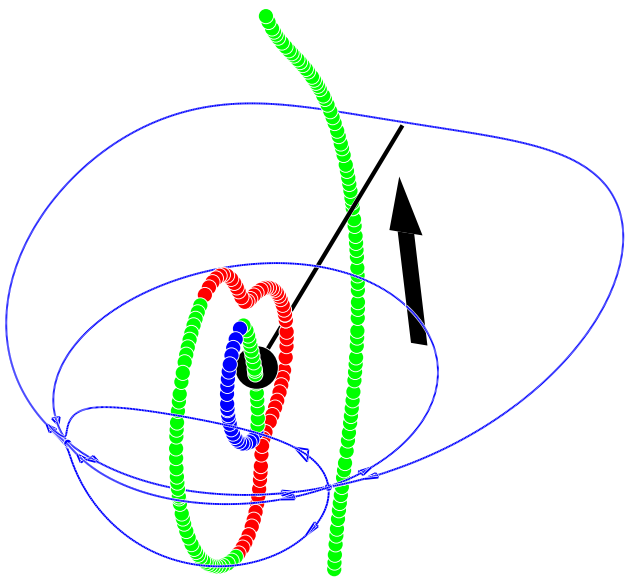

Fig. 11 Asymptotic lines connecting the (3,±1) points in the CO_2 molecule

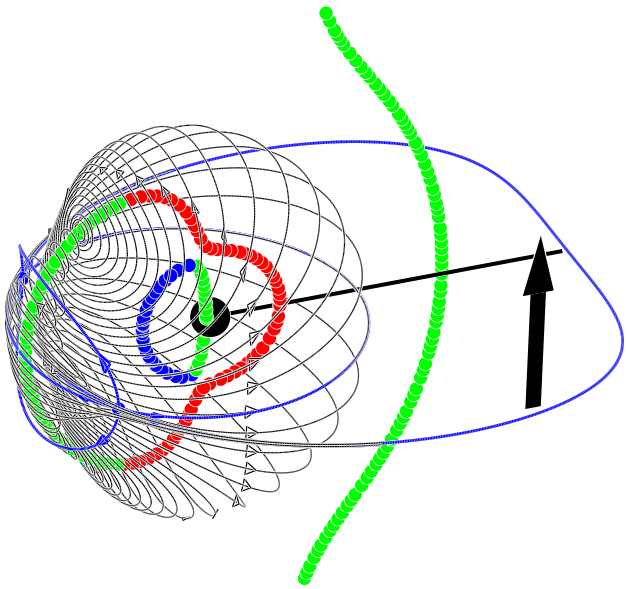

Fig. 12 Toroidal regime in the neighbourhood of an oxygen atom in the CO_2 molecule. The figure shows the small-size of the diamagnetic portion

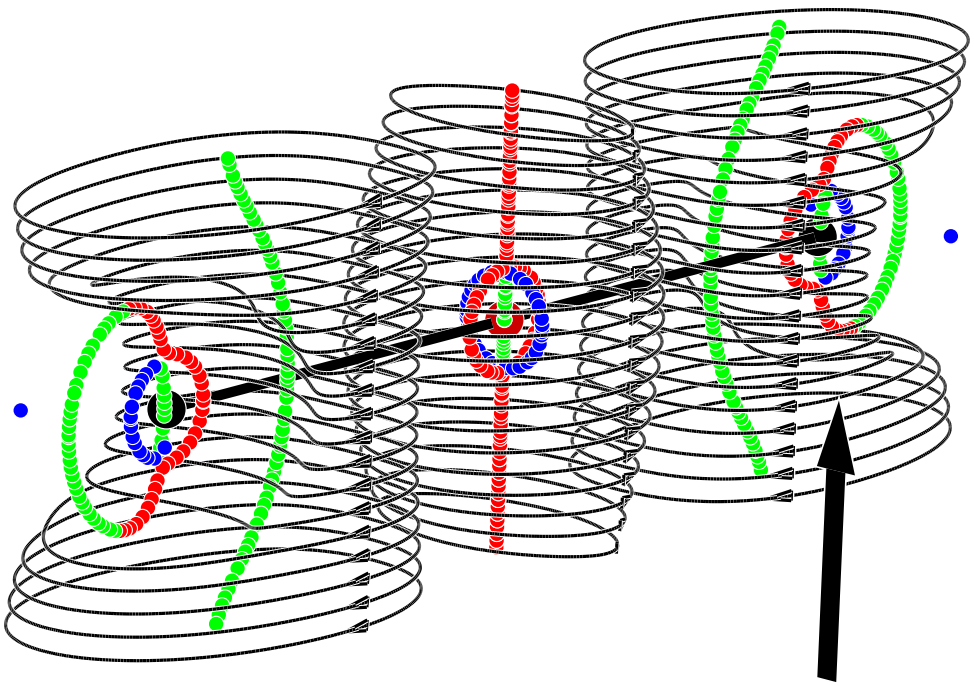

Fig. 13 The central paratropic flow in the basin of the carbon atom and the diamagnetic vortices about the oxygen atoms in the CO_2 molecule

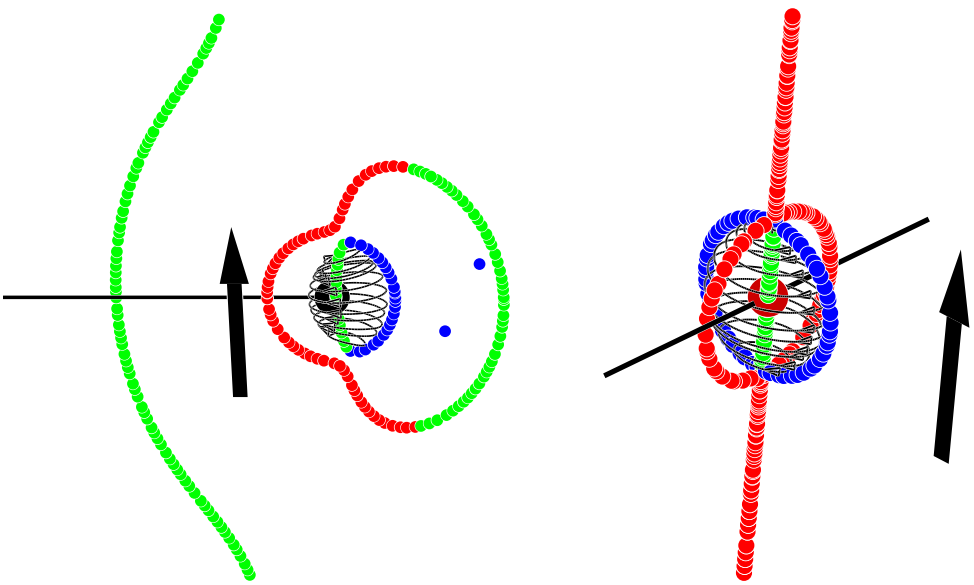

Fig. 14 Magnified view of the diamagnetic vortices about the oxygen and carbon nuclei in the CO_2 molecule

mark the intersection of the plane of the nuclei with (1) the cylindrical separatrix of the diamagnetic AV crossing the C–O bonds; (2) the spherical separatrix of the torus. Figs. 11 and 12 show that the diamagnetic portion of toroidal flow is confined within a very small region.

Streamline maps with different scale are displayed in Fig. 10 to visualize the current density field. The bottom-right magnified view of the basin of the carbon atom shows the SPs at the intersection of the five SLs forming the central cage in Fig. 9 with the σ_h plane containing the bond axis. Two saddles and two paramagnetic vortices appear at orthogonal directions on either side of the central diamagnetic vortex. In Fig. 10, the bottom-left blow-up of the region nearby one of the oxygen nucleus shows the intersection of the toroidal flow with the σ_h plane. The paramagnetic vortex corresponding to the outer loop in Fig. 9 is much bigger than the diamagnetic, visible above as single closed trajectory flanked by the (3,±1) saddle-nodes. These isolated SPs look like saddles on the plot plane, see Fig. 11.

4 Conclusions

This study shows that simple and compact spatial models of the quantum-mechanical current density $\mathbf{J}^{\mathbf{B}}$ induced by a uniform magnetic field in the electron cloud of small molecules can be constructed by stagnation graphs collecting isolated points and continuous sets of points at which the modulus $|\mathbf{J}^{\mathbf{B}}|$ vanishes. The heuristic value of stagnation graphs for discovering and describing the essentials of the current density field via a minimum atlas of streamline maps in different regions of molecular domain was proved. The theoretical methods outlined in this work can easily be extended to larger systems, in which more complicated types of flow are likely to occur, to understand molecular magnetotropicity, and to rationalize magnetic susceptibilities and nuclear magnetic shieldings. They may also serve to investigate peculiar features of magnetic response that have so far received little attention, for instance, discovery of orbital electronic anapole moments associated with toroidal vortices, and their manifestation in nuclear magnetic resonance spectroscopy.

Acknowledgments Financial support to the present research from the Italian MURST (Ministero dell'Università e della Ricerca Scientifica e Tecnologica), via FAR and PRIN funds, is gratefully acknowledged.

References

1. Madelung E (1926) Z Phys 40:322
2. Schrödinger E (1926) Ann Phys (Leipzig) 81:109
3. de Broglie L (1926) C R Acad Sci (Paris) 183:447
4. de Broglie L (1927) C R Acad Sci (Paris) 184:273
5. Landau LD, Lifshitz EM (1981) Quantum mechanics. Pergamon Press, Oxford
6. Hamilton W (1833) On a general method of expressing the paths of light, and of the planets, by the coefficients of a characteristic function. Dublin University Rev:795–826
7. Hamilton W (1834) On the application to dynamics of a general mathematical method previously applied to optics. British Association Report, London, pp 513–518
8. Landau L (1941) J Phys USSR 5:71
9. London F (1945) Rev Mod Phys 17:310
10. Bohm D (1952) Phys Rev 85:166
11. Bohm D (1952) Phys Rev 85:180
12. Halpern O (1952) Phys Rev 87:389
13. Bohm D (1952) Phys Rev 87:389
14. Epstein ST (1953) Phys Rev 89:319
15. Bohm D (1953) Phys Rev 89:319
16. Bohm D (1953) Phys Rev 89:458
17. Bohm D, Hiley BJ, Kaloyerou PN (1987) Phys Rep 144:321
18. Bohm D, Peat FD (2000) Science, order, and creativity, 2nd edn. Routledge, London
19. Bialynicki-Birula I, Bialynicka-Birula Z (1971) Phys Rev D 3:2410
20. Hirschfelder JO, Christoph AC (1974) J Chem Phys 61:5435
21. Hirschfelder JO, Goebel CJ, Bruch LW (1974) J Chem Phys 61:5456
22. Hirschfelder JO, Tang KT (1976) J Chem Phys 64:760
23. Hirschfelder JO, Tang KT (1976) J Chem Phys 65:470
24. Lopreore CL, Wyatt RE (1999) Phys Rev Lett 82:5190
25. Derrickson SW, Bittner ER, Kendrick BK (2005) J Chem Phys 123:054107
26. Deckert D-A, Dürr D, Pickl P (2007) J Phys Chem A 111:10325
27. Dey BK, Askar A, Rabitz H (1998) Chem Phys Lett 297:247
28. Dey BK, Rabitz H, Askar A (2000) Phys Rev A 61:043412
29. Hu XG, Rabitz H, Askar A (2000) Phys Rev D 61:5967
30. Mayor FS, Rabitz H, Askar A (1999) J Chem Phys 111:2423
31. McLafferty F (2002) J Chem Phys 117:10474
32. Stevens RM, Nipscomb W (1964) J Chem Phys 40:2238
33. Stevens RM, Lipscomb WN (1964) J Chem Phys 41:3710
34. Hegstrom RA, Lipscomb WN (1966) J Chem Phys 45:2378
35. Laws EA, Stevens RM, Lipscomb WN (1971) J Chem Phys. 54:4269
36. Lazzeretti P, Zanasi R (1983) J Am Chem Soc 105:12
37. Lazzeretti P, Zanasi R (1982) J Chem Phys 77:3129
38. Lazzeretti P, Rossi E, Zanasi R (1984) Int J Quantum Chem XXV:929
39. Lazzeretti P, Rossi E, Zanasi R (1984) Int J Quantum Chem XXV:1123
40. Keith TA, Bader RFW (1993) Chem Phys Lett 210:223
41. Keith TA, Bader RFW (1993) J Chem Phys 99:3669
42. Bader RFW, Keith TA (1993) J Chem Phys 99:3683
43. Keith TA, Bader RFW (1996) Can J Chem 74:185
44. Bader RFW, Keith TA (1996) Int J Quantum Chem 60:373
45. Pelloni S, Faglioni F, Zanasi R, Lazzeretti P (2006) Phys Rev A 74:012506
46. Pelloni S, Lazzeretti P (2007) Theor Chem Acc 117:903
47. Pelloni S, Lazzeretti P, Zanasi R (2007) J Phys Chem A 111:3110
48. Pelloni S, Lazzeretti P, Zanasi R (2007) J Phys Chem A 111:8163
49. Pelloni S, Lazzeretti P (2007) Theor Chem Acc 118:89
50. Pelloni S, Lazzeretti P (2008) J Phys Chem A 112:5175
51. Pelloni S, Lazzeretti P (2008) J Chem Phys 128:194305
52. Kutzelnigg W, Fleischer U, Schindler M (1990) The IGLO method:Ab initio calculation and interpretation of NMR chemical shifts and magnetic susceptibilities. In: NMR, basic principles and progress, vol 23, Springer, Berlin, pp 165–262
53. Kutzelnigg W, van Wüllen C, Fleischer U, Franke R, van Mourik T (1993) In: Tossell JA (ed) Nuclear magnetic shielding and molecular structure, vol 386 of NATO ASI Series C. Kluwer Academic Publishers, Dordrecht, pp 141–161
54. Fleischer U (1992) Anwendungen der IGLO Methode und ihre Interpretation. Ruhr-Universität Bochum, Ph.D Thesis, in German
55. Havenith RWA, Fowler PW, Steiner E (2003) Chem Phys Lett 371:276
56. Fowler PW, Baker J, Lillington M (2007) Theor Chem Acc 118:123
57. Ligabue A, Pincelli U, Lazzeretti P, Zanasi R (1999) J Am Chem Soc 121:5513
58. Lazzeretti P (2000) In: Emsley JW, Feeney J, Sutcliffe LH (eds) Progress in nuclear magnetic resonance spectroscopy, vol 36. Elsevier, Amsterdam, pp 1–88
59. Kutzelnigg W (1980) Isr J Chem 19:193
60. Schindler M, Kutzelnigg W (1982) J Chem Phys 76:1919
61. Fleischer U, Kutzelnigg W, Lazzeretti P, Mühlenkamp V (1994) Am Chem Soc 116:5298
62. Lin Y-C, Jusélius J, Sundholm D, Gauss J (2005) J Chem Phys 122:214308
63. Johansson MP, Jusélius J (2005) Lett Org Chem 2:469
64. Johansson MP, Jusélius J, Sundholm D (2005) Angew Chem Int Ed Engl 44:1843

65. Bast R, Jusélius J, Saue T (2008) Chem Phys published on line, doi:10.1016/j.chemphys.2008.10.040
66. Frisch MJ, Trucks GW et al (2003) Gaussian 2003, Revision B.05. Gaussian Inc, Pittsburgh
67. Geertsen J (1989) J Chem Phys 90:4892
68. Geertsen J (1991) Chem Phys Lett 179:479
69. Geertsen J (1992) Chem Phys Lett 188:326
70. Lazzeretti P, Malagoli M, Zanasi R (1994) Chem Phys Lett 220:299
71. Coriani S, Lazzeretti P, Malagoli M, Zanasi R (1994) Theor Chim Acta 89:181
72. Zanasi R (1996) J Chem Phys 105:1460
73. van Duijneveldt FB (1971) Gaussian basis sets for the atoms H–Ne for use in molecular calculations. Research report RJ 945, IBM
74. Lazzeretti P, Malagoli M, Zanasi R (1991) Technical report on project sistemi informatici e calcolo parallelo. Research report 1/67, CNR
75. Gomes JANF (1983) Phys Rev A 28:559
76. Gomes JANF (1983) J Chem Phys 78:4585
77. Gomes JANF (1983) J Mol Struct (Theochem) 93:111
78. Gomes JANF, Mallion RB (2001) Chem Rev 101:1349
79. Milnor JW (1997) Topology from the differentiable viewpoint. University of Virginia Press, Charlottesville
80. Guillemin V, Pollack A (1974) Differential topology. Prentice-Hall, Englewood Cliffs
81. Hirschfelder JO (1977) J Chem Phys 67:5477
82. Reyn JW (1964) Z Angew Math Physik 15:540
83. Khriplovich IB (1991) Parity nonconservation in atomic phenomena. Gordon & Breach, Oxford
84. Faglioni F, Ligabue A, Pelloni S, Soncini A, Lazzeretti P (2004) Chem Phys 304:289
85. Pelloni S, Lazzeretti P (in preparation)
86. Gomes JANF (1983) J Chem Phys 78:3133
87. Zanasi R, Lazzeretti P, Malagoli M, Piccinini F (1995) J Chem Phys 102:7150